# Real Time Microfluidic Blood Counting System for PET and SPECT Preclinical Pharmacokinetic Studies – Supplemental Data –

Laurence Convert[1,2,3], Réjean Lebel[1], Suzanne Gascon[1], Réjean Fontaine[3], Jean-François Pratte[3], Paul Charette[2,3], Vincent Aimez[2,3], Roger Lecomte[1]

[1]Sherbrooke Molecular Imaging Centre of CRCHUS and Department of Nuclear Medicine and Radiobiology, Université de Sherbrooke, Sherbrooke, QC, Canada
[2]Laboratoire Nanotechnologies Nanosystèmes (LN2) - CNRS UMI-3463, Université de Sherbrooke, Sherbrooke, QC, Canada
[3]Institut Interdisciplinaire d'Innovation Technologique (3IT), Université de Sherbrooke, Sherbrooke, QC, Canada

## SECTION 1 - OVERVIEW OF MICROFLUIDICIC BLOOD COUNTING SYSTEM

### System Description

The proposed microfluidic blood counting system consists of two separate hardware modules that can be used next to an imaging scanner (Manuscript Fig. 1). The detection unit includes the microfluidic chip, a signal processing board, and a miniature peristaltic pump (P625/900.133, Instech Laboratories Inc., Plymouth Meeting, USA). The pump accommodates speed from 4 to 3300 µL/min depending on the tubing used. Pumping speed was measured to range from 5 to 90 µL/min with 0.51 mm ID tubing and 20 to 290 µL/min with 0.79 mm ID tubing from PharMed® (Saint-Gobain). A 2-cm thick lead shield protects the detector from radioactivity in the animal and the injection syringe. Four 9 V batteries placed in series supply the detector reverse bias voltage ($V_{bias}$ = -36 V). The signal processing board, powered by an external AC-DC converter (PSA-46-301, Phihong, Fremont, USA), shapes and amplifies the signal from a linear array of typically eight 2 × 2 $mm^2$ silicon *p-i-n* photodiodes connected in parallel and outputs differential analog pulses to the control unit (Supplemental Fig. 1A). Based on an integrated 16-channel LabPET™ charge sensitive preamplifier (*1*), the design can be easily upgraded to multichannel data acquisition for monitoring different parts of the microfluidic chip with more complex functionalities.

The control unit includes electronics for counting radiation pulses, controlling the blood drawing speed, and USB communication based on a Silicon Labs 8151 microcontroller, all powered by the USB port. This unit digitizes the analog pulses from the detector unit and allows adjustment of the lower discriminator level to ensure that the optimal threshold is set for each experiment (Supplemental Fig. 1B). The differential communication between the two units ensures the low noise operation required for processing very weak signals from *p-i-n* photodiodes. The microfluidic detector front-end is vulnerable to electromagnetic interference often present in a scanner environment. The microfluidic chip and signal processing board must be properly grounded to a common mass at all times and sometimes be electromagnetically shielded from the animal and scanner using a metal enclosure.

A user friendly control software interface is used to set experiment parameters, display the blood time-activity curve in real time and process the recorded data. Based on the previously developed catheter-based microvolumetric beta blood counter (µBC) software (*2*), this software version was upgraded to allow USB communication and pump control.

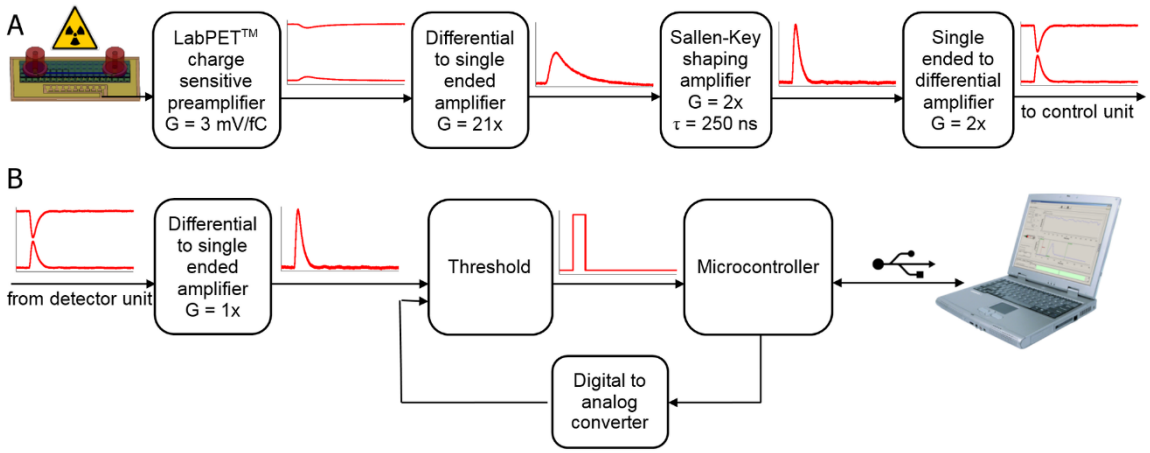


**Supplemental Figure 1**: Electronic block diagrams of the detection unit (**A**) and control unit (**B**). Sample waveforms at the output of each block illustrate the typical signal resulting from the detection of a positron.

## Microfluidic Channel Fabrication Process

After dicing a linear array of 2 × 2 $mm^2$ silicon *p-i-n* photodiodes from a wafer, the die was passivated with 300 nm of $SiO_2$, and the channel floor was added by photolithography of KMPR (1-10 µm), an epoxy-based photoresist (Microchem, Newton, USA), to expose the diodes anode top contacts. Gold traces were added to bring the contacts away from the microchannel. KMPR channel walls were added by photolithography. A previously wet-etched glass channel roof was bonded with a thin KMPR layer. Nanoports (N126H, Upchurch Scientific, Oak Harbor, USA) were added on the glass cover for fluidic connections. A gold-plated custom-made PCB was used to connect diodes in parallel. The die back-contact formed the common cathode and eight top-contact anodes were wire-bonded to the PCB anode traces. The KMPR microchannel walls were passivated with Bovine Serum Albumin (BSA) to increase the chip hemocompatibility. BSA is a plasma protein strongly adsorbed at the KMPR surface, preventing adhesion of clotting proteins like fibrinogen. BSA at 10 mg/mL in phosphate buffer saline was flowed through the channels at 2 µL/min for 2 h. This simple but effective passivation was performed after the microchannel packaging.

## Operation with Animals

Operation with animals requires special care to avoid coagulation and to minimize connections dead volume. The PE10 arterial line, pre-filled with heparinized saline (0.9%, 40 U/mL), was usually connected to a pre-filled PE10 catheter interfaced to the microfluidic system using a small piece of PE50 tubing. The PE10 catheters can thus be considered to form a continuous line between the animal and microfluidic system. It is not really possible to flush the catheter line after the junction is made, but heparin filling of the tubing was found sufficient to prevent clotting. Initially, the peristaltic pump prevents blood from seeping into the catheter, but as soon as the pump is started it should not be stopped to avoid clotting. One way to flush the entire line following unexpected interruption would be to invert the peristaltic pump while drawing saline from the end of the line. However, if clotting occurs within the microfluidic system, there is no real way to clean the microchannel and the chip would have to be replaced.

Whole-blood compatibility of lab-on-a-chip devices is another matter of concern (*3*). Experiments with mice reported in this work showed good hemocompatibility of the microfluidic blood counting system as no blood clotting was observed for experiments of up to 40 min at low rate (10 µL/min). Furthermore, the same device was used repeatedly on different animals after a wash using an enzymatic cleaner (Asepti-Zyme, Merck Santé Animale, Québec, Canada) at the end of experiments and a new BSA treatment before subsequent experiments. The reliability of this process was confirmed over a period of several months.

## SECTION 2: MICROFLUIDIC BLOOD COUNTING SYSTEM ASSESSMENT FOR DEAD TIME, SENSITIVITY TO BACKGROUND RADIOACTIVITY AND SAMPLE TEMPERATURE

### Dead Time

The dead time and linearity of the microfluidic counting system were determined experimentally by recording the decay of a $^{11}$C source placed inside the detection volume (130 kBq to 130 Bq). The theoretical count rate, $n$ (cps), was computed from the measured count rate, $m$ (cps), at the end of the acquisition considering the system sensitivity and no dead time. The paralysable, $\tau_P$ (s) (Eq. S1), and non-paralysable, $\tau_{NP}$ (s) (Eq. S2), dead times (*4*) were then fitted with OriginPro 8.6 (OriginLab, Northampton, USA) following:

$$m = n \times e^{-n\times\tau_P}, \qquad \text{Eq. S1}$$

$$m = \frac{n}{(1+n\times\tau_{NP})}. \qquad \text{Eq. S2}$$

For the application in blood counting, a system can be considered linear for dead time losses below 1% ($\varepsilon = m/n > 99\%$).

The measured and expected count rates are illustrated in Supplemental Fig. 2. The system dead time was found to be 1.8 µs for both the paralysable and non-paralysable models. The linearity was better than 1% up to 10 kcps and better than 2% up to 16 kcps. As a comparison, the mouse blood activity following a high 37 MBq bolus injection is about 20 kBq/µL, corresponding to 6.2 kcps for the isotope with the maximum detection efficiency ($^{11}$C). As radioactive concentration in rat blood is usually less than in mouse, no correction for dead-time would be required for typical small animal experiments.

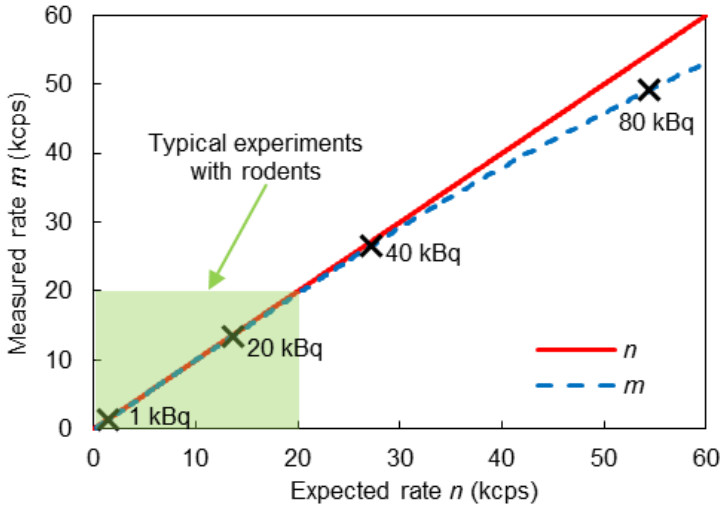


**Supplemental Figure 2:** Measured ($m$) and expected ($n$) count rate for a $^{11}$C liquid source. A few data points were added on the measured rate curve, indicating the range of measured count rates corresponding to the actual $^{11}$C activity in the detection volume.

### Background Sensitivity

In typical applications, the microfluidic detector is placed close to an animal injected with 30-60 MBq while measuring a few kBq in the blood detection volume. The efficiency of the detector module lead shielding was assessed by recording the count rate with a 60 MBq source of $^{18}$F placed 5 cm away from the detector unit. The system count rate was found to be no higher than the default background count rate set

before the experiment (typically 5 cps). Hence, the shielding appears to be fully adequate for utilizing the counter just next to the animal with negligible background effect on AIF measurements.

### Sample Temperature

The influence of the sample temperature on the detector electronic noise was assessed by withdrawing water at 20 to 50°C inside the microfluidic blood counting system through a 20-cm-long PE10 tubing and recording the count rate. The detection threshold was adjusted to record 5 cps background count rate while withdrawing water at 20°C.

The system background count rate was not different with a sampling volume at room temperature and up to 50ºC (5 cps). It was therefore concluded that the microfluidic blood counting system would not be affected by animal blood temperature.

## SECTION 3: CORRECTION FOR DISPERSION

Dispersion in a catheter is usually modeled by a single exponential and corrected by deconvolution with parameters previously estimated by measuring the system response to a step function (*5*,*6*) or fitted on the measured input function, $AIF_m$ (*7*). In the present work, we chose to fit the dispersion time constant, $\tau_{disp}$, on the AIF using Matlab. An undispersed input function, $AIF_u$, was first created using a rectangular function depicting the radiotracer injection in the vascular compartment convoluted with a bi-exponential clearance accounting for rapid tissue uptake and biological half-life following (*8*):

$$AIF_u = rect\left(\frac{t-(T_{max}-T_{inj})}{T_{inj}}\right) \otimes \left(K_1 exp^{-t/T_1} + K_2 exp^{-t/T_2}\right), \quad \text{Eq. S1}$$

where $T_{max}$ (s) is the time delay to the maximum in $AIF_m$, $T_{inj}$ (s) is the injection duration and $K_1$, $T_1$, $K_2$, and $T_2$ are clearance parameters. A dispersed input function, $AIF_d$, was then calculated using a monoexponential function with a default $\tau_{disp}$:

$$AIF_d = (a.AIF_u) \otimes exp^{-\ln(2).t/\tau_{disp}}, \quad \text{Eq. S2}$$

where $a$ is the amplitude of the function. Finally, the six parameters $K_1$, $T_1$, $K_2$, $T_2$, $a$, and $\tau_{disp}$ were fitted to minimize the mean least square error between $AIF_d$ and $AIF_m$. The measured input function corrected for dispersion was then obtained using Equation S1 with $K_1$, $T_1$, $K_2$, $T_2$, and $a$ fitted on $AIF_m$ and $\tau_{disp} = 0$. It should be noted that to facilitate the curve fitting, the statistical noise inherent in any radioactivity measurement was usually reduced by smoothing $AIF_m$ (moving average, 10 seconds).

## SECTION 4: $^{11}$C-ACETATE PHARMACOKINETIC MODEL

The tissue uptake of $^{11}$C-acetate in the myocardium can be described using a three-compartment kinetic model by the following equation (*9*):

$$C_t(t) = [A_1.exp(-(k_2+k_3)t) + A_2.exp(-k_4 t)] \otimes C_p(t) + vC_{tot}(t), \quad \text{Eq. S3}$$

with $A_1 = K_1k_2/(k_2+k_3)$ and $A_2 = K_1k_3/(k_2+k_3)$, where $K_1$, $k_2$, $k_3$, and $k_4$ are the rate constants, $v$ is the blood volume, $C_t$ is the myocardial TAC, $C_p$ is the $^{11}$C-acetate arterial blood concentration and $C_{tot}$ is the total $^{11}$C arterial blood concentration including metabolites. The constants $K_1$ and $k_2$ respectively provide indexes of myocardial blood flow (MBF) and myocardial oxygen consumption ($MVO_2$) when applied to the cardiac muscle. The model also includes a correction for the presence of $^{11}$C-$CO_2$ in blood, the metabolite of $^{11}$C-acetate, following:

$$C_p(t) = \left[1 - a_0\left(1 - exp^{-t.ln(2)/m}\right)\right].C_{tot}(t), \quad \text{Eq. S4}$$

where $a_0$ and $m$ are parameters fitted by the kinetic model in addition to the rate constants.

## REFERENCES


1. Pratte J-F, Robert S, De Geronimo G, et al. Design and performance of 0.18-μm CMOS charge preamplifiers for APD-based PET scanners. *IEEE Trans Nucl Sci*. 2004;51:1979-1985.

2. Convert L, Morin-Brassard G, Cadorette J, Archambault M, Bentourkia M, Lecomte R. A new tool for molecular imaging: the microvolumetric beta blood counter. *J Nucl Med*. 2007;48:1197-1206.

3. Rosen Y, Gurman P. MEMS and microfluidics for diagnostics devices. *Curr Pharm Biotechnol*. 2010;11:366-75.

4. Knoll GF. *Radiation Detection and Measurement*. 3rd Ed. New York: John Wiley and Sons, 2000, p. 122.

5. Iida H, Kanno I, Miura S, Murakami M, Takahashi K, Uemura K. Error analysis of a quantitative cerebral blood flow measurement using $H_2{}^{15}O$ autoradiography and positron emission tomography, with respect to the dispersion of the input function. *J Cereb Blood Flow Metab*. 1986;6:536-545.

6. Kanno I, Iida H, Miura S, et al. A system for cerebral blood flow measurement using an $H_2{}^{15}O$ autoradiographic method and positron emission tomography. *J Cereb Blood Flow Metab*. 1987;7:143-153.

7. Meyer E. Simultaneous correction for tracer arrival delay and dispersion in CBF measurements by the $H_2{}^{15}O$ autoradiographic method and dynamic PET. *J Nucl Med*. 1989;30:1069-1078.

8. McGrath DM, Bradley DP, Tessier JL, Lacey T, Taylor CJ, Parker GJM. Comparison of model-based arterial input functions for dynamic contrast-enhanced MRI in tumor bearing rats. *Magn Reson Med*. 2009;61:1173-1184.

9. Bentourkia M, Croteau É, Langlois R, et al. Cardiac studies in rats with $^{11}$C-acetate and PET: a comparison with $^{13}$N-ammonia. *IEEE Trans Nucl Sci*. 2002;49:2322-2327.